biomolecules

MDPI

Article

Lactobacillus crispatus FY121-Derived Extracellular Vesicles Suppress HPV-Positive Cervical Cancer Cells and Activate RIG-I/MAVS/IRF3 Signaling

Guoding Cao [1,2,†], Shuang Liang [3,†], Meng Yuan [1,2], Chongyao Xue [1,2], Mingyang Ding [1,2], Luyi Li [1,2] and Yong Fang [1,2,*]

[1] Department of Microbiology, School of Basic Medical Sciences, Harbin Medical University, Harbin 150081, China
[2] Heilongjiang Province Key Laboratory of Immunity & Infection, Harbin 150081, China
[3] Virology Laboratory, Harbin Center for Disease Control and Prevention, Harbin 150056, China
* Correspondence: yong.fang@ems.hrbmu.edu.cn; Tel.: +86-138-4508-5386
† These authors contributed equally to this work.

Abstract

High-risk human papillomavirus (HPV) infection is the major cause of cervical cancer (CC), and viral oncogenes E6 and E7 contribute to tumor progression by promoting malignant transformation and impairing innate immune responses. Extracellular vesicles (EVs) derived from beneficial bacteria have emerged as potential regulators of host cellular functions. However, their role in HPV-associated cervical cancer remains unclear. In this study, we isolated and characterized extracellular vesicles derived from *Lactobacillus crispatus* FY121 (LcEVs) and investigated their effects on HPV-positive cervical cancer cell lines. LcEVs were efficiently internalized by HPV16-positive SiHa and HPV18-positive HeLa cells and significantly suppressed cell proliferation, migration, and invasion. Furthermore, LcEVs reduced HPV E6 and E7 expression at both the transcriptional and protein levels. Mechanistically, LcEV treatment was associated with increased RIG-I/MAVS/IRF3 signaling and enhanced IFN-β transcription and secretion. Transcriptomic analysis further revealed broad alterations in immune-related and cellular functional programs following LcEV treatment. In a co-injection xenograft model, LcEVs reduced tumor establishment and early outgrowth of HPV-positive cervical cancer cells and were accompanied by increased RIG-I/MAVS/IRF3 signaling in tumor tissue. Proteomic profiling identified diverse functional proteins within LcEVs, providing potential molecular candidates underlying their biological effects. Together, these results show that LcEVs suppress the malignant phenotypes of HPV-positive cervical cancer cells and are accompanied by activation of nucleic acid sensing and type I interferon signaling in vitro and in vivo. The identity of the active vesicular cargo and its causal contribution to these effects remain to be established, and bacterial EVs are highlighted as candidate immunomodulatory agents for HPV-related malignancies.

Keywords: *Lactobacillus crispatus*; extracellular vesicles; RIG-I; HPV; cervical cancer

Check for updates

Academic Editor: Joe S. Mymryk

Received: 27 September 2026
Revised: 22 October 2026
Accepted: 23 October 2026
Published: 26 October 2026

Copyright: © 2026 by the authors. Licensee MDPI, Basel, Switzerland. This article is an open access article distributed under the terms and conditions of the Creative Commons Attribution (CC BY) license.

1. Introduction

Cervical cancer (CC) is the fourth most common malignancy among women worldwide, with almost all cases attributable to persistent infection with human papillomavirus (HPV). HPV infection is also a major etiological factor for vaginal cancer, vulvar cancer, anal

cancer, and oropharyngeal cancer, particularly cancers arising from the base of the tongue and tonsils [1,2]. HPV (family Papillomaviridae) is a small, non-enveloped virus containing a circular double-stranded DNA genome. Persistent infection with high-risk HPV types is considered the primary cause of CC. Among the various HPV genotypes, HPV16 and HPV18 are the most prevalent and oncogenic types, accounting for approximately 70% of cervical cancer cases [3]. The HPV genome consists of three major regions: the early gene-encoding region (E), the late gene-encoding region (L), and the long control region (LCR) [4]. The E6 and E7 oncoproteins of high-risk HPV drive malignant transformation by promoting uncontrolled cell proliferation, angiogenesis, invasion and metastasis, sustained telomerase activation, and resistance to apoptosis and growth inhibition [4]. Therefore, E6 and E7 are considered key oncogenic drivers of HPV infection and represent major targets for therapeutic HPV vaccine development. Although preventive HPV vaccination, surgery, radiotherapy, and chemotherapy have achieved significant advances in controlling HPV-associated diseases, the global burden of HPV-related malignancies remains substantial. In particular, effective therapeutic strategies targeting HPV pathogenesis and virus-induced immune evasion remain limited [5].

Innate immunity is an essential defense mechanism that protects the host against pathogen infection [6]. Pattern recognition receptors (PRRs) recognize pathogen-associated molecular patterns (PAMPs) and subsequently induce the production of type I interferons and other inflammatory cytokines [6,7]. During HPV infection, viral persistence is closely associated with the suppression of host innate immune sensing mechanisms [8,9]. Previous studies have demonstrated that multiple viral proteins encoded by high-risk HPV can interfere with nucleic acid sensing pathways, including the cGAS-STING-mediated DNA sensing pathway and the RIG-I-like receptor-mediated RNA sensing pathway, thereby limiting IRF3 activation and reducing IFN-β production, which facilitates viral persistence and immune evasion [10–12]. Therefore, restoring nucleic acid sensing signaling and type I interferon responses within the HPV-induced immunosuppressive environment represents an important direction for the development of therapeutic strategies against HPV-associated malignancies.

Although HPV infection is associated with impaired nucleic acid sensing, restoring innate immune activation through alternative immune pathways may provide a potential therapeutic strategy. Retinoic acid-inducible gene I (RIG-I)-like receptors (RLRs) are key cytosolic RNA sensors that recognize immunostimulatory RNA molecules and initiate type I interferon responses through the MAVS-TBK1-IRF3 signaling cascade [13,14]. Notably, RIG-I-mediated immune activation is not limited to the recognition of exogenous viral RNA; aberrant accumulation of endogenous double-stranded RNA (dsRNA) can also trigger RIG-I-dependent interferon responses. In a model of FUS mutant amyotrophic lateral sclerosis, cytoplasmic dsRNA accumulation induced increased RIG-I expression and activated the TBK1-IRF3 pathway, thereby promoting the expression of interferon-stimulated genes, suggesting that RIG-I can sense RNA signals from different sources and regulate innate immune responses [15]. In melanoma models, specific RIG-I agonists consisting of 5′-triphosphate short RNA activated the RIG-I-MAVS signaling axis, induced antitumor immune responses, and reduced tumor progression [16]. Therefore, utilizing exogenous RNA signals to reactivate RIG-I-mediated innate immune responses may represent a potential strategy for restoring immune function in HPV-associated tumors.

Extracellular vesicles (EVs) are released by organisms across all domains of life and are defined as lipid bilayer-enclosed particles that cannot replicate on their own, and membrane vesicles are produced by both Gram-negative and Gram-positive bacteria, including Gram-positive *lactobacilli* [17,18]. In Gram-negative bacteria, vesicle formation has been linked to outer membrane blebbing, whereas in Gram-positive bacteria, which

lack an outer membrane, vesicles are thought to arise from the cytoplasmic membrane, and the underlying mechanisms remain incompletely defined [19,20]. Bacterial EVs carry proteins, lipids, nucleic acids, and metabolites derived from the producing cell and act as vehicles for bacterium–bacterium and bacterium–host communication [21,22]. Because these vesicles are internalized by host cells and deliver cargo into the cytoplasm, they are increasingly recognized as modulators of host signaling in infection, inflammation, and cancer [23,24]. In the vaginal niche, EVs released by commensal *lactobacilli* interact with the cervicovaginal epithelium and modulate host cell responses [25,26]. Notably, bacterial EVs can transfer bacterial RNA into host cells, and vesicle-associated RNA is recognized by the cytosolic RNA sensor RIG-I to induce type I interferon responses [27]. However, whether EVs released by vaginal *Lactobacillus* species regulate tumor cell intrinsic RNA sensing and whether such regulation affects HPV-driven cervical cancer progression remain largely unexplored.

The present study aimed to investigate whether LcEVs could regulate HPV-associated cervical cancer progression and to explore the underlying mechanisms. We isolated and characterized LcEVs and found that they could be efficiently internalized by HPV-positive cervical cancer cells. Functional studies demonstrated that LcEVs suppressed HPV E6/E7 expression and inhibited the proliferation, migration, and invasion of cervical cancer cells. Mechanistically, LcEVs activated the RIG-I/MAVS/IRF3 signaling axis, leading to increased IFN-β expression and secretion, and their inhibitory effects on tumor growth were further validated in a xenograft model. In addition, proteomic analysis revealed that LcEVs contain multiple potentially functional proteins, providing a basis for further investigation of their immunomodulatory mechanisms.

2. Materials and Methods

2.1. LcEV Collection and Characterization

Lactobacillus crispatus FY121 was originally isolated from vaginal secretions collected from healthy women and deposited in the China General Microbiological Culture Collection Center (CGMCC, Beijing, China) under accession number CGMCC No. 28788. For extracellular vesicle preparation, *L. crispatus FY121* was inoculated into De Man, Rogosa, and Sharpe (MRS) broth and cultured overnight at 37 °C. The bacterial culture was centrifuged at 4500× *g* for 15 min at 4 °C to remove bacterial cells, and the resulting supernatant was carefully collected and passed through a 0.45 μm membrane filter to further eliminate residual cells and large particulate material. The filtered culture supernatant was transferred into ultracentrifugation tubes and centrifuged at 120,000× *g* for 60 min at 4 °C. After removal of the supernatant, the resulting pellet was gently resuspended in sterile phosphate-buffered saline (PBS) and subjected to a second ultracentrifugation at 120,000× *g* for 60 min at 4 °C to reduce soluble and non-vesicular contaminants. The final pellet was designated LcEVs and resuspended in sterile PBS for subsequent characterization and experiments. The protein content of the LcEV preparations was estimated by measuring absorbance at 280 nm using a NanoDrop 2000 spectrophotometer (Thermo Fisher Scientific, Waltham, MA, USA). For morphological characterization, LcEVs were fixed with 2.5% glutaraldehyde, loaded onto 300 mesh copper grids, negatively stained with 2% uranyl acetate, and examined using transmission electron microscopy (TEM; Hitachi, Japan). Particle size distribution and particle concentration were determined by nanoparticle tracking analysis using a ZetaView instrument (Particle Metrix, Meerbusch, Germany) at 26 °C. Samples were diluted 3000-fold in PBS to bring the particle number per frame into the working range of the instrument, and three measurement cycles at eleven positions were recorded (ZetaView software 8.05.14 SP7; 4626 particles tracked). Both the measured concentration of the diluted sample and the dilution-corrected concentration of the preparation are reported.

2.2. LcEV Proteomic Analysis

Proteomic profiling of LcEVs was performed by Jingjie PTM Biolab (Hangzhou, China) using four-dimensional label-free (4D-LF) proteomics. Briefly, purified LcEV samples were lysed in 8 M urea, followed by protein extraction and concentration determination using a bicinchoninic acid (BCA) assay. Extracted proteins were enzymatically digested with trypsin, and the resulting peptides were subjected to liquid chromatography–tandem mass spectrometry (LC–MS/MS) analysis. Peptide separation was performed using a NanoElute ultra-high-performance liquid chromatography system, followed by detection on a timsTOF Pro mass spectrometer (Bruker Daltonics, Bremen, Germany) operated in parallel accumulation serial fragmentation (PASEF) mode.

The raw MS/MS data were processed using MaxQuant software (version 1.6.15.0). Protein identification was performed against the *Lactobacillus crispatus* UniProt database (*Lactobacillus_crispatus*_47770_UP_20220418_seqkit. fasta; 25,128 sequences) supplemented with a reverse decoy database and common contaminant database. Trypsin/P was selected as the digestion enzyme with a maximum of two missed cleavages allowed. The peptide length was set to a minimum of seven amino acids. Carbamidomethylation of cysteine was defined as a fixed modification, while methionine oxidation and protein N-terminal acetylation were considered variable modifications. Mass tolerance was set to 20 ppm for precursor ions in both the first and main searches, and 20 ppm for fragment ions. False discovery rates (FDRs) for peptide-spectrum matches (PSMs) and protein identification were controlled at <1%.

2.3. Cell Culture

Cervical cancer cell lines, including HPV16-positive SiHa and HPV18-positive HeLa cells, were obtained from the Department of Microbiology, Harbin Medical University (Harbin, China); these lines correspond to ATCC HTB-35 (SiHa) and ATCC CCL-2 (HeLa). Cells were cultured in Dulbecco's modified Eagle's medium (DMEM; Thermo Fisher Scientific, Waltham, MA, USA) supplemented with 10% fetal bovine serum (CB FBS, catalog no. AUS-01E-02), 100 U/mL penicillin, and 0.1 mg/mL streptomycin (Beyotime, Shanghai, China). Cells were maintained at 37 °C in a humidified atmosphere containing 5% CO_2. The FBS used in this study was commercially available sterile fetal bovine serum. The serum was not subjected to ultracentrifugation-based extracellular vesicle depletion; therefore, the potential presence of trace bovine-derived extracellular vesicles in the culture medium cannot be completely excluded.

2.4. LcEV Labeling and Cellular Uptake Assay

Observation of internalization of LcEVs by cervical cancer cell lines. The RNA of LcEVs was labeled with ExoGlow™-RNA EV Labeling Kit (System Biosciences, Palo Alto, CA, USA). LcEVs were mixed with the incubation buffer, then the fluorescent dye was added, and the mixture was incubated in the dark at 37 °C for 1 h. Cervical cancer cells were then added to the labeled LcEVs and incubated for 24 h at 37 °C. ExoGlow™-Membrane EV Labeling Kit (System Biosciences, Palo Alto, CA, USA) labeled the membranes of LcEVs. The reaction buffer was mixed with the fluorescent dye, and the resulting mixture was loaded with LcEVs and incubated at room temperature away from light, for 1 h. Next, cervical cancer cells were incubated with the labeled LcEVs for 24 h at 37 °C. The nuclei of the cells were stained by using a Hoechst and observed under a Cell Voyager CV1000 confocal microscope (Yokogawa, Yokohama, Japan).

2.5. Cell Proliferation Assay

Cells were seeded into 96-well plates with 100 µL of culture medium per well. After 16 h of incubation, the medium was replaced with fresh medium containing different concentrations of LcEVs (200, 300, and 400 µg/mL), corresponding to $5 \times 10^{\hat{}10}$, $7.5 \times 10^{\hat{}10}$, and $1 \times 10^{\hat{}11}$ particles/mL). After 48 h of co-culture at 37 °C, 10 µL of Cell Counting Kit-8 (CCK-8, Beyotime, Shanghai, China) solution was added to each well, followed by incubation at 37 °C for 1.5 h. Finally, the absorbance at 450 nm was measured by an enzyme marker (Molecular Devices, San Jose, CA, USA).

2.6. Migration and Invasion Analysis

In cell migration assays, 200 µL of serum-free DMEM was added to a Transwell chamber (Corning, Cambridge, MA, USA) with 8.0 µm pore membranes along with either 400 µg/mL LcEVs or PBS. The lower chamber was supplemented with DMEM containing 10% FBS. For cell invasion assay, serum-free DMEM was added to the invasion chamber (Corning, Cambridge, MA, USA), as well as to the lower chamber, and hydrated at 37 °C for 2 h. After that, 200 µL of cells in serum-free DMEM was treated with 400 µg/mL LcEVs or PBS at the same time. DMEM containing 10% FBS was added to the lower chamber. After 48 h of incubation, migrated and invaded cells were fixed with 4% paraformaldehyde (Biosharp, Hefei, China). The cells were then rinsed twice with PBS and stained with a 0.1% crystal violet (Biosharp, Hefei, China) for 15 min. Stained cells were observed using an inverted light microscope (Leica, Wetzlar, Germany), and five fields of view were randomly selected for counting.

2.7. Transcriptome Sequencing (RNA-Seq) and Bioinformatics Analysis

Total RNA was extracted from cultured cells using TRIzol reagent according to the manufacturer's instructions. RNA concentration was measured using a Qubit RNA Assay Kit with a Qubit 2.0 Fluorometer (Life Technologies, Carlsbad, CA, USA), and RNA integrity was evaluated using the RNA Nano 6000 Assay Kit with an Agilent Bioanalyzer system. RNA samples with sufficient quality were used for library construction. Sequencing libraries were prepared using the NEBNext® Ultra™ RNA Library Preparation Kit for Illumina® sequencing (New England Biolabs, Ipswich, MA, USA) according to the manufacturer's protocol. The constructed libraries were sequenced on an Illumina HiSeq platform. Raw sequencing data were processed using standard bioinformatics pipelines. Gene set enrichment analysis (GSEA) was performed to evaluate the enrichment of predefined gene sets and biological pathways. Gene sets with an absolute normalized enrichment score (NES) > 1 and nominal p value < 0.05 were considered significantly enriched. GSEA enrichment plots, network visualization, and rose plots were generated using the online bioinformatics platform (https://www.bioinformatics.com.cn; accessed on 4 May 2026) [28].

2.8. Protein–Protein Docking

The 3D structures of protein TrxA were obtained from the alpha-fold protein database (https://alphafold.com), with UniProt ID A0A109DE80, while the 3D structure of protein RIG-I was obtained from the PDB protein database (https://www.rcsb.org/), with a PDB ID of 7mk1. Auto dock Tools were used to eliminate water molecules and extract small molecules such as inhibitors and ions in order to create the 3D structure of the protein. This entails retaining the primary structure of the protein and converting it into PDB format. In order to predict protein–protein docking, the proteins were imported into ZDOCK 3.0.2 separately, and rigid docking was used for protein-wide docking prediction. The docking results were analyzed and plotted using PyMol.

2.9. Quantitative Real-Time PCR

Total RNA was collected using Trizol reagent, and the obtained total RNA was reverse transcribed to cDNA using PrimeScript™ RT Master Mix (Takara, Kusatsu, Shiga, Japan). RT-qPCR was performed using SYBR Premix Ex Taq (Takara, Kusatsu, Shiga, Japan) with 45 thermal cycles of 95 °C for 10 s, 60 °C for 20 s, and 72 °C for 20 s. The relative mRNA expression of each gene was calculated by the $2^{-\Delta\Delta CT}$ method. GAPDH was employed as an internal control. All primer sequences are presented in Table 1.

Table 1. Primer sequences used in RT-qPCR.

Gene	Forward Sequence (5′ → 3′)	Reverse Sequence (5′ → 3′)
16 E6	GAACAGCAATACAACAAACCG	CCACCGACCCCTTATATTATG
16 E7	CAGCTCAGAGGAGGAGGATG	CACAACCGAAGCGTAGAGTC
18 E6	ATCCAACACGGCGACCCTACAA	CTGGATTCTATGTCACGAGCAAT
18 E7	GCATGGACCTAAGGCAACA	CTCGTCGGGCTGGTAAAT
RIG-I	AACCAGAATTATCCCAACCGAT	TCCCCTTAGTAGAGCAAATCTGTA
MAVS	CAGCAAGAGACCAGGGACC	TGTTGTAGGGGATGCTGTGG
IRF3	TTCATTGTAGGCTCCTGGGC	CACACAGAACCAGAGGGCAT
IFN-β	ACGCCGCATTGACCATCTAT	GTCTCATTCCAGCCAGTGCT
GAPDH	AACTTTCGATGGTAGTCGCCG	CCTTGGATGTGGTAGCCGTTT

2.10. Western Blot

Total cellular proteins were extracted using RIPA lysis buffer (Beyotime, Shanghai, China), and protein concentrations were determined using a BCA Protein Assay Kit (Beyotime, Shanghai, China). Equal amounts of protein samples were separated by SDS-PAGE and transferred onto nitrocellulose membranes. The membranes were blocked with 5% skimmed milk in TBST for 2 h at room temperature and then incubated overnight at 4 °C with primary antibodies diluted in TBST. The following primary antibodies were used: rabbit monoclonal antibody against HPV16/18 E6 (Ab70, 1:100, Abcam, Cambridge, MA, USA); mouse monoclonal antibody against HPV16 E7 (clone 28-0006, 1:100, Thermo Fisher Scientific, Waltham, MA, USA); mouse monoclonal antibody against HPV18 E7 (SC-365035, 1:100, Santa Cruz Biotechnology, Dallas, TX, USA); rabbit monoclonal antibody against MAVS (#3993, 1:1000, Cell Signaling Technology, Danvers, MA, USA); rabbit polyclonal antibody against RIG-I (20566-1-AP, 1:1000, Proteintech, Wuhan, China); rabbit polyclonal antibody against phospho-IRF3 (p-IRF3) (29528-1-AP, 1:1000, Proteintech, Wuhan, China); rabbit polyclonal antibody against IRF3 (11312-1-AP, 1:1000, Proteintech, Wuhan, China); mouse monoclonal antibody against β-actin (AC026, 1:5000, ABclonal, Wuhan, China); and rabbit monoclonal antibody against β-tubulin (AC008, 1:2000, ABclonal, Wuhan, China). After washing with TBST, membranes were incubated with horseradish peroxidase (HRP)-conjugated secondary antibodies (A0208 and A0216, 1:2000, Beyotime, Shanghai, China) for 1 h at room temperature. Protein signals were detected using an enhanced chemiluminescence (ECL) detection kit (Biosharp, Hefei, China), and band intensities were quantified using ImageJ 1.53e (National Institutes of Health, Bethesda, MD, USA).

2.11. Animal Experiments

Female BALB/c nude mice aged 4 weeks were obtained from Charles River Laboratories (Beijing, China). Animals were maintained under specific pathogen-free (SPF) conditions with sterilized bedding, food, and water and were acclimatized before tumor inoculation. All animal procedures were reviewed and approved by the Institutional Animal Care and Use Committee of Harbin Medical University (approval no. HMUIRB2026037) and were conducted in accordance with institutional animal welfare guidelines and the

ARRIVE guidelines. The mice were randomly allocated into four groups (n = 7 per group): (1) SiHa cell group, (2) SiHa cell plus LcEV group, (3) HeLa cell group, and (4) HeLa cell plus LcEV group. For tumor establishment, SiHa or HeLa cells (2×10^6 cells per mouse) were mixed with LcEVs to a final concentration of 400 μg EV protein/mL, and the mixture was injected subcutaneously in a total volume of 150 μL immediately after mixing, corresponding to 60 μg of LcEV protein per mouse. Control groups received the same number of cells mixed with an equal volume of PBS. Tumor growth and general health status were monitored regularly, and tumor dimensions were measured using a digital caliper. Tumor volume was calculated according to the formula tumor volume = 0.5 × length × width^2. The experiment was terminated when tumors reached the predefined endpoint criteria according to institutional animal welfare requirements. At the endpoint, mice were anesthetized and euthanized, and tumors were excised, photographed, weighed, and measured. Tumor tissues were subsequently fixed, embedded, and sectioned for further histological and molecular analyses.

2.12. Immunohistochemistry (IHC)

Paraffin-embedded tumor tissues were sectioned and subjected to IHC staining. Briefly, tissue sections were deparaffinized in xylene, rehydrated through a graded ethanol series, and treated with 3% hydrogen peroxide for 30 min at room temperature to block endogenous peroxidase activity. After antigen retrieval and blocking of non-specific binding with skim milk solution, sections were incubated overnight at 4 °C with primary antibodies against MAVS, RIG-I, and phospho-IRF3. The primary antibodies used were as follows: rabbit monoclonal antibody against MAVS (Cat#3993, 1:1000, Cell Signaling Technology, Danvers, MA, USA); rabbit polyclonal antibody against RIG-I (Cat#20566-1-AP, 1:1000, Proteintech, Wuhan, China); and rabbit polyclonal antibody against phospho-IRF3 (p-IRF3) (Cat#29528-1-AP, 1:1000, Proteintech, Wuhan, China). After washing with PBS, sections were incubated with HRP-conjugated anti-rabbit secondary antibody at 37 °C for 30 min. Immunoreactivity was visualized using 3,3′-diaminobenzidine (DAB) chromogen and counterstained with hematoxylin. Images were captured using a light microscope (Leica Microsystems, Wetzlar, Germany). For each tumor sample, five randomly selected fields were photographed under identical magnification and acquisition conditions. The percentage of positively stained area was quantified using ImageJ 1.53e (National Institutes of Health, Bethesda, MD, USA).

2.13. Enzyme-Linked Immunosorbent Assay (ELISA)

IFN-β in culture supernatants was measured using a human IFN-β ELISA kit (E-EL-H0085; Elabscience, Wuhan, China) following the manufacturer's protocol, after SiHa and HeLa cells had been stimulated with 400 μg EV protein/mL LcEVs for 48 h.

2.14. Statistical Analysis

Each cell-based experiment was performed in three independent biological replicates. The xenograft experiment used seven mice per group. Data are presented as mean ± SD. Comparisons between two groups were performed with unpaired two-tailed Student's *t*-tests, and comparisons among more than two groups were performed with one-way ANOVA followed by Tukey's multiple comparison test. Tumor growth curves were compared with two-way repeated-measures ANOVA. $p < 0.05$ was considered statistically significant. Analyses were performed with GraphPad Prism 9.5 (GraphPad Software, San Diego, CA, USA). Each figure legend states the number of replicates and the statistical test used.

3. Results

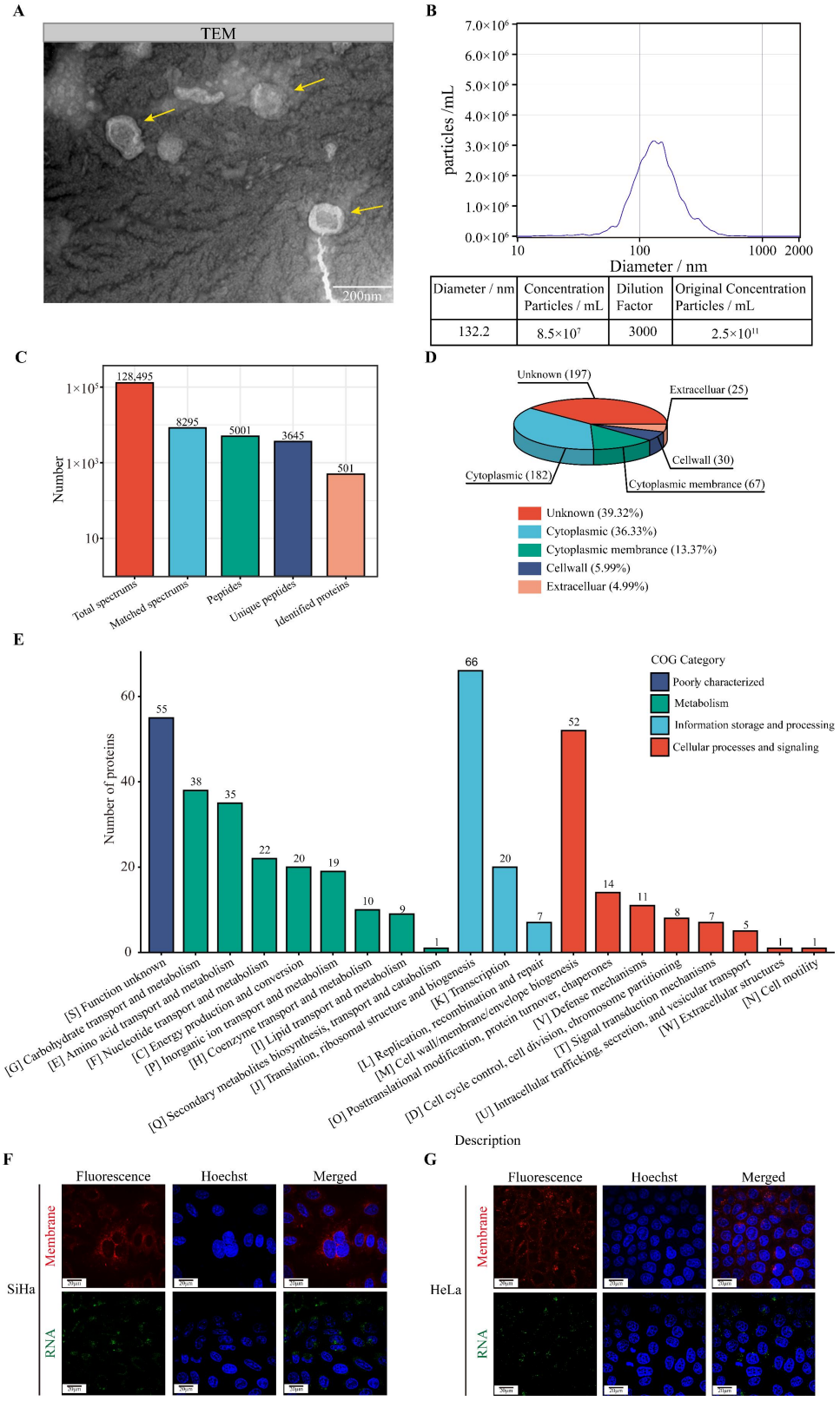
3.1. Characterization, Functional Annotation, and Cellular Uptake of LcEVs Derived from Lactobacillus crispatus FY121

To characterize the extracellular vesicles released by *L. crispatus* FY121 (LcEVs), LcEVs were isolated and subjected to morphological and physicochemical characterization. TEM analysis revealed that LcEVs exhibited spherical or oval vesicle-like structures with variable sizes (Figure 1A). Additional TEM images obtained from different fields of view further supported these morphological observations (Figure S1A). Quantitative analysis of vesicle diameters from the TEM images revealed a mean diameter of 130.5 nm and a median diameter of 136.2 nm (Figure S1B). The NTA of the LcEV preparation showed a median particle diameter (X50) of 132.2 nm (Figure 1B). The sample was diluted 3000-fold to bring the particle number per frame into the working range of the instrument. The measured concentration of the diluted sample was 8.5×10^7 particles/mL, and the corresponding concentration of the preparation was 2.5×10^{11} particles/mL. Notably, the median diameter measured by TEM was comparable to the median particle diameter (X50) of 132.2 nm determined by NTA. To further investigate the potential functional components of LcEVs, proteomic analysis was performed. A total of 501 proteins were identified from LcEVs (Figure 1C). The identified proteins were annotated to *L. crispatus*, and no proteins from the common contaminant database were retained, which argues against contamination with medium or mammalian proteins. Subcellular localization analysis showed that 182 proteins were predicted to be localized in the cytoplasm, 67 proteins in the cytoplasmic membrane, 30 proteins in the cell wall, and 25 proteins in extracellular regions, while 197 proteins were assigned to unknown locations (Figure 1D). This distribution is consistent with a preparation enriched in bacterial membrane vesicles. Functional classification using the Cluster of Orthologous Groups of Proteins (COG) database revealed that LcEV-associated proteins were mainly involved in cellular metabolism, including carbohydrate, amino acid, and nucleotide transport and metabolism, as well as information storage and processing processes, including replication, recombination, transcription, and translation. In addition, several identified proteins were associated with cellular processes and signaling, including membrane biogenesis, posttranslational modification, and cellular regulation (Figure 1E). These results suggest that LcEVs contain diverse proteins potentially involved in metabolic regulation and cellular signaling processes. To determine whether LcEVs could be internalized by cervical cancer cells, LcEVs were labeled using ExoGlow Membrane EV Labeling Kit and ExoGlow RNA EV Labeling Kit and incubated with SiHa and HeLa cells. Confocal microscopy analysis demonstrated that both membrane-labeled and RNA-labeled EV signals were detected within SiHa and HeLa cells after 24 h of incubation (Figure 1F,G). These findings indicate that LcEVs can be efficiently taken up by HPV-positive cervical cancer cells.

3.2. LcEVs Suppress the Proliferation, Migration, and Invasion of Cervical Cancer Cells

To determine the biological effects of LcEVs on cervical cancer cells, the proliferative capacity of SiHa and HeLa cells was evaluated using the CCK-8 assay following treatment with different concentrations of LcEVs. Compared with the control group, LcEV treatment resulted in a concentration-dependent reduction in cell viability. The strongest inhibitory effect on the proliferation of both SiHa and HeLa cells was observed at a concentration of 400 μg EVs protein/mL, corresponding to $1 \times 10^{\hat{}11}$ particles/mL (Figure 2A,B). The effects of LcEVs on cell migration and invasion were further assessed using Transwell assays. Compared with untreated cells, LcEV treatment significantly reduced the migratory and invasive abilities of both SiHa and HeLa cells (Figure 2C–F). Together, these results

demonstrate that LcEVs suppress the proliferation, migration, and invasion abilities of HPV-positive cervical cancer cells.



Diameter / nm	Concentration Particles / mL	Dilution Factor	Original Concentration Particles / mL
132.2	8.5×10^{7}	3000	2.5×10^{11}

Figure 1. Characterization, functional annotation, and cellular uptake of LcEVs derived from *Lactobacillus crispatus* FY121. (**A**) Representative TEM images showing the morphology of LcEVs. Yellow arrows indicate vesicle structures. The images were acquired at a magnification of 30,000×, Scale bar = 200 nm. (**B**) NTA of LcEVs showing the size distribution. The sample was diluted 3000-fold; the

measured concentration of the diluted sample was 8.5×10^7 particles/mL and the concentration of the preparation was 2.5×10^{11} particles/mL. The value at the modal peak is the height of the size distribution and is not the total particle concentration. (**C**) Summary of proteomic identification results of LcEVs, including total spectra, matched spectra, identified peptides, unique peptides, and identified proteins. (**D**) Subcellular localization analysis of LcEV-associated proteins. (**E**) Functional classification of LcEV proteins based on the Cluster of Orthologous Groups (COG) database. (**F**,**G**) Confocal microscopy analysis of LcEV uptake by SiHa and HeLa cells. EV membranes were labeled using ExoGlow Membrane EV Labeling Kit, and EV-associated RNA was labeled using ExoGlow RNA EV Labeling Kit. Cells were analyzed after 24 h of co-incubation.

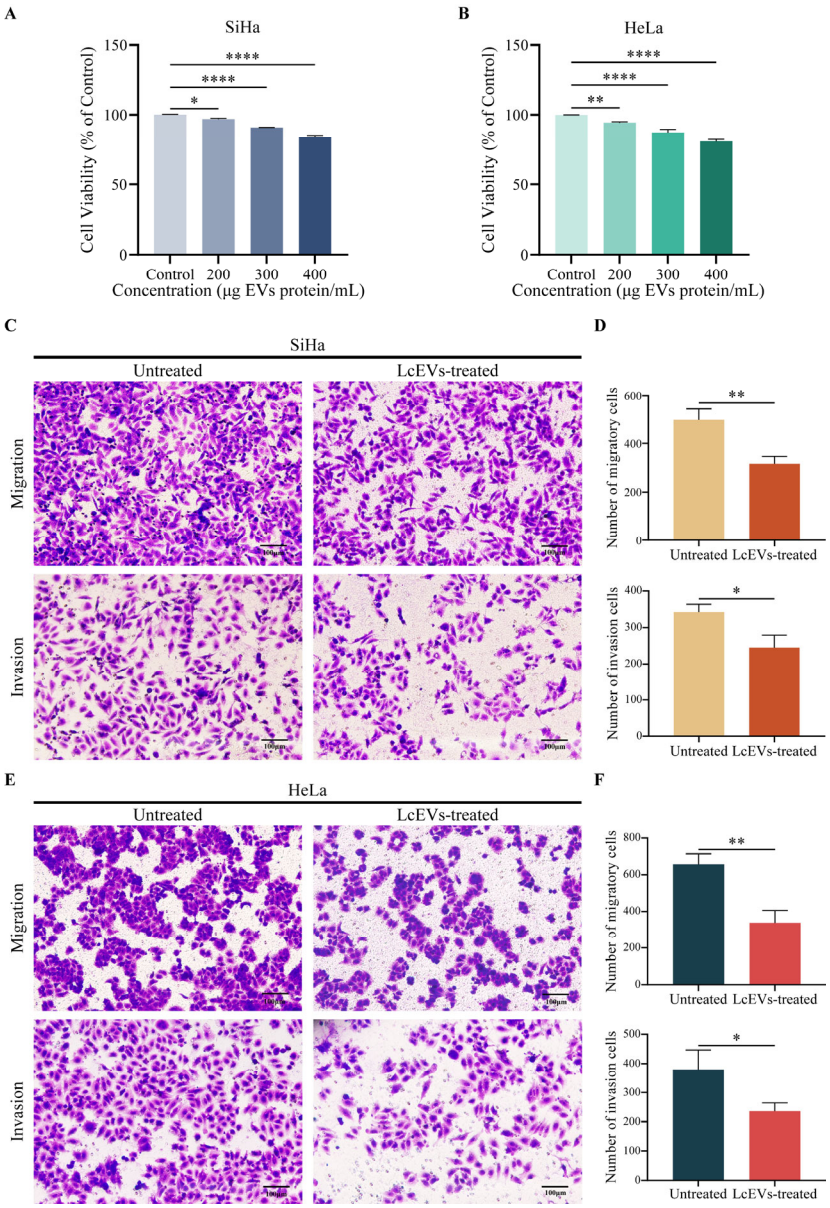


Figure 2. LcEVs suppress the proliferation, migration, and invasion of cervical cancer cells. (**A**,**B**) Cell viability analysis of SiHa and HeLa cells treated with different concentrations of LcEVs using the CCK-8 assay. (**C**) Representative images of transwell migration and invasion assays in SiHa cells following LcEV treatment. (**D**) Quantitative analysis of migrated and invaded SiHa cells. (**E**) Representative images of transwell migration and invasion assays in HeLa cells following LcEV treatment. (**F**) Quantitative analysis of migrated and invaded HeLa cells. Data are presented as mean ± SD of three independent experiments. One-way ANOVA with Tukey's multiple comparison test was used for panels (**A**,**B**), and unpaired two-tailed Student's *t* tests were used for panels D and F. * $p < 0.05$, ** $p < 0.01$, **** $p < 0.0001$.

3.3. LcEVs Suppress the Expression of HPV16 and HPV18 E6 and E7 Oncogenes in Cervical Cancer Cells

To determine whether LcEV treatment affects HPV oncogene expression, HPV16-positive SiHa cells and HPV18-positive HeLa cells were treated with 400 μg EV protein/mL LcEVs for 48 h, and the expression levels of E6 and E7 were evaluated at both the mRNA and protein levels using qRT-PCR and Western blot analysis. In SiHa cells, LcEV treatment significantly reduced the mRNA expression levels of HPV16 E6 and E7 compared with the untreated group (Figure 3A,B). Consistently, Western blot analysis showed that the protein levels of HPV16 E6 and E7 were markedly decreased following LcEV treatment (Figure 3C,D). Similarly, in HPV18-positive HeLa cells, LcEV treatment resulted in a significant reduction in HPV18 E6 and E7 mRNA expression (Figure 3E,F). The protein expression levels of HPV18 E6 and E7 were also decreased after LcEV treatment. These results demonstrate that LcEV treatment suppresses the expression of HPV16 and HPV18 E6 and E7 at both the transcriptional and protein levels in HPV-positive cervical cancer cells.

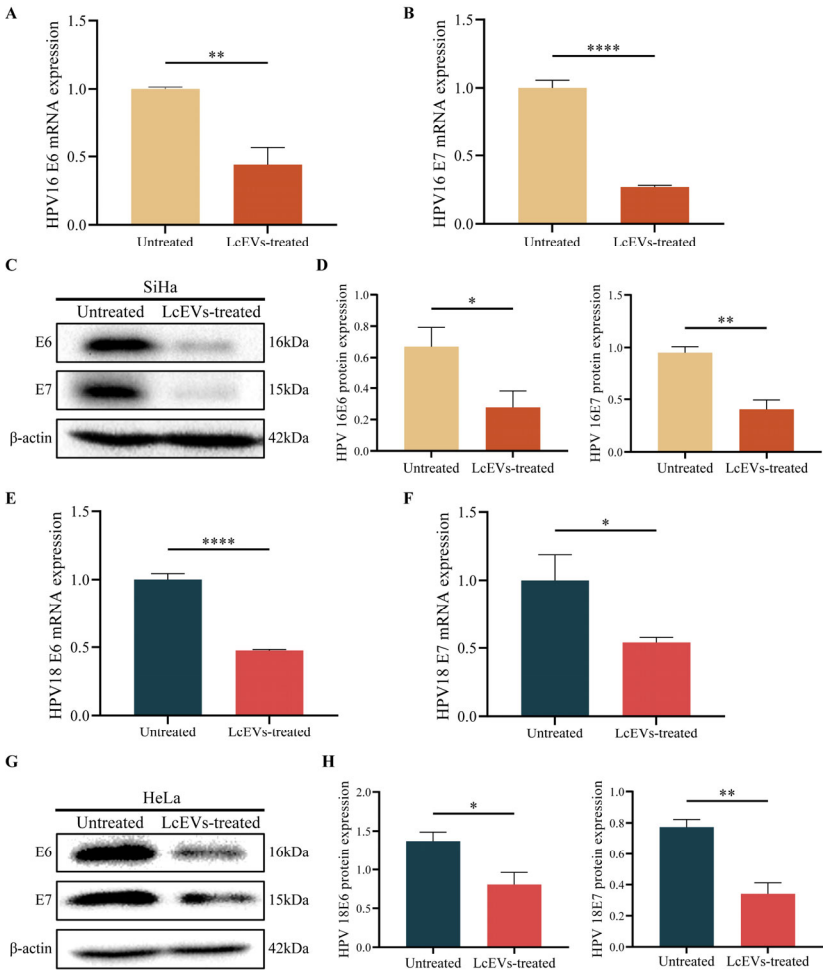


Figure 3. LcEVs suppress the expression of high-risk HPV E6 and E7 oncogenes in cervical cancer cells. (**A**,**B**) Relative mRNA expression levels of HPV16 E6 and E7 in SiHa cells following LcEV treatment determined by qRT-PCR. (**C**) Western blot analysis of HPV16 E6 and E7 protein expression in SiHa cells after LcEV treatment. (**D**) Quantitative analysis of HPV16 E6 and E7 protein expression levels in SiHa cells. (**E**,**F**) Relative mRNA expression levels of HPV18 E6 and E7 in HeLa cells following LcEV treatment determined by qRT-PCR. (**G**) Western blot analysis of HPV18 E6 and E7 protein expression in HeLa cells after LcEV treatment. (**H**) Quantitative analysis of HPV18 E6 and E7 protein expression levels in HeLa cells. Data are presented as mean ± SD. Statistical analyses were by Student's *t*-tests. * $p < 0.05$, ** $p < 0.01$, **** $p < 0.0001$. Original images of Figure 3C,G can be found in Supplementary File S1.

3.4. LcEV Treatment Induces IFN-β Expression and Activates the RIG-I/MAVS/IRF3 Signaling Axis in HPV-Positive Cervical Cancer Cells

To investigate whether LcEV treatment activates RLR signaling, we first treated HPV16-positive SiHa cells and HPV18-positive HeLa cells with 400 μg EV protein/mL LcEVs for 48 h and then examined IFN-β mRNA expression and protein secretion. Compared with the untreated group, LcEV treatment significantly increased IFN-β mRNA expression in SiHa cells (Figure 4A). Consistent with the mRNA results, ELISA analysis showed that LcEV treatment significantly enhanced IFN-β secretion in the culture supernatant (Figure 4B). Next, we evaluated the expression of key genes and proteins involved in the RIG-I signaling pathway. In SiHa cells, LcEV treatment significantly increased the mRNA expression levels of RIG-I, MAVS, and IRF3 (Figure 4C). Western blot analysis further demonstrated that LcEV treatment increased RIG-I and MAVS protein expression and promoted IRF3 phosphorylation (p-IRF3) (Figure 4D,E). Similar increases in IFN-β mRNA expression and protein secretion, together with activation of the RIG-I/MAVS/IRF3 signaling axis, were observed in HeLa cells following LcEV treatment (Figure 4F–J).

Following validation of the RLR signaling response induced by LcEVs, transcriptome sequencing was further performed to analyze the overall transcriptional changes associated with LcEV treatment. GSEA of GO biological processes revealed alterations in multiple cellular function and immune-related biological processes. Among these processes, sensory perception of chemical stimulus, ion transport, regulation of membrane potential, and cilium movement were enriched following LcEV treatment. Gene sets associated with negative regulation of leukocyte-mediated immunity also showed enrichment tendency (Figure 4K). GSEA of KEGG pathways showed that several metabolic and cellular maintenance-related pathways were negatively enriched after LcEV treatment, including ribosome, proteasome, and pathways associated with DNA replication and repair (Figure 4L). Meanwhile, glycosphingolipid biosynthesis, complement and coagulation cascades, and several immune-related signaling pathways were positively enriched (Figure 4M). These transcriptomic results indicate that LcEV treatment is associated with alterations in transcriptional programs related to cellular functions, metabolism, and immune regulation.

Collectively, these results show that LcEV treatment is accompanied by activation of the RIG-I/MAVS/IRF3 axis and increased IFN-β production in HPV-positive cervical cancer cells, and that transcriptional programs related to immune regulation and cellular function are altered.

3.5. LcEVs Suppress Tumor Progression In Vivo

To examine whether LcEVs affect tumor establishment and early growth in vivo, SiHa or HeLa cells were co-injected with LcEVs into the flanks of BALB/c nude mice, and RIG-I signaling was examined in the resulting tumors. Compared with the untreated group, LcEV treatment significantly suppressed tumor growth in SiHa xenografts. Tumor volume increased at a slower rate during treatment, and the final tumor weight was significantly reduced in the LcEV-treated group compared with the untreated group (Figure 5A–C). Next, we examined the expression of RIG-I signaling-related molecules in tumor tissues by IHC staining. In SiHa xenografts, LcEV treatment resulted in increased expression of RIG-I, MAVS, and p-IRF3 compared with untreated tumors. Quantitative analysis further demonstrated a significant increase in the percentage of RIG-I-, MAVS-, and p-IRF3-positive cells following LcEV treatment (Figure 5D–I). To further determine whether these effects were consistent in another HPV-positive cervical cancer model, HPV18-positive HeLa xenografts were established. Similar to the SiHa model, LcEV treatment significantly inhibited tumor growth and reduced tumor weight in HeLa xenografts (Figure 5J–L). IHC analysis further showed that LcEV treatment increased RIG-I, MAVS, and p-IRF3

expression in HeLa tumor tissues, accompanied by an increased proportion of positive cells (Figure 5M–R). Collectively, these results show that co-injection of LcEVs with tumor cells reduced tumor establishment and early outgrowth in both xenograft models and was accompanied by activation of the RIG-I/MAVS/IRF3 axis in tumor tissue. Because LcEVs were co-injected with the cells, this design does not test the treatment of established tumors.

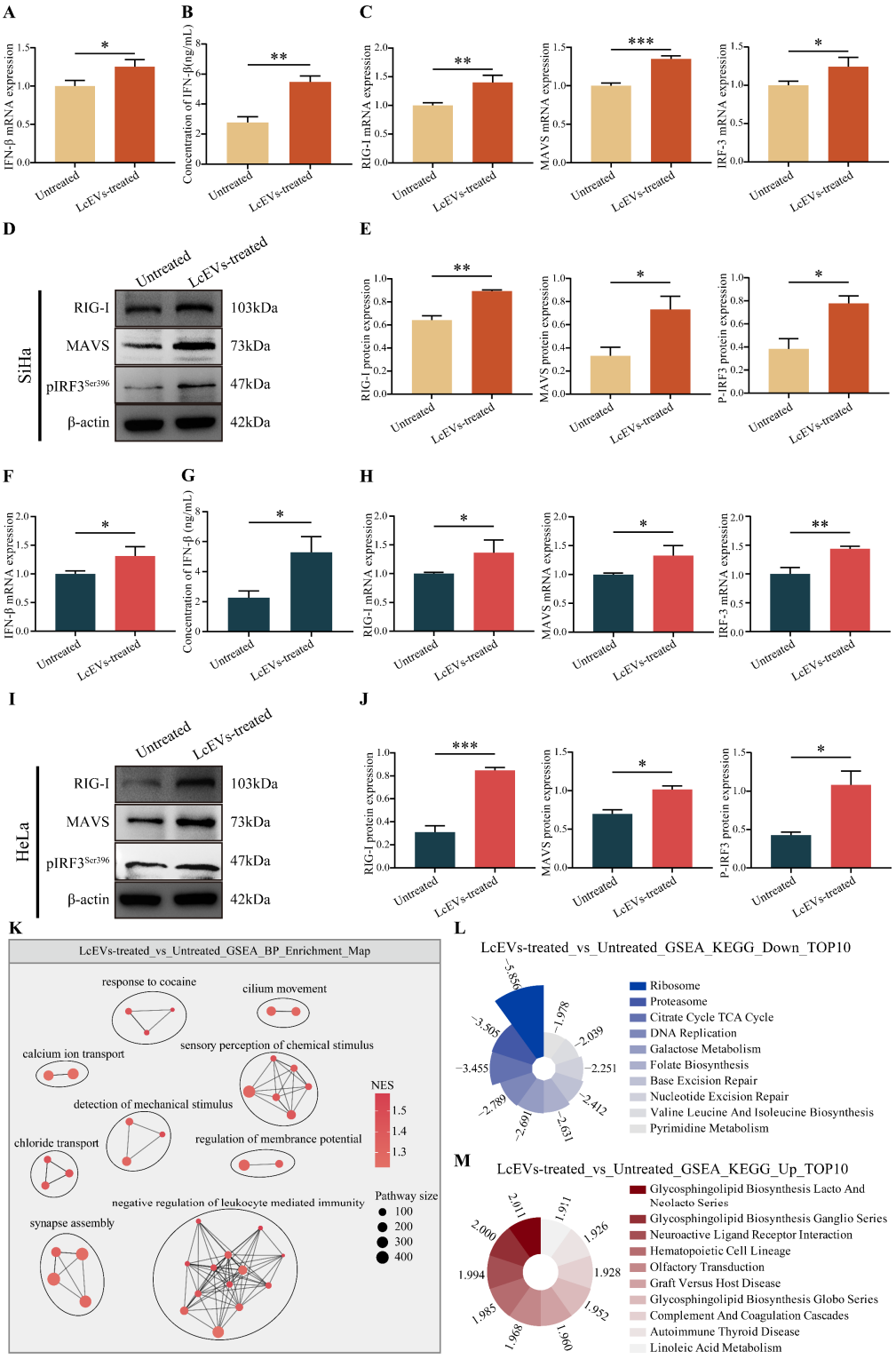


Figure 4. LcEV treatment induces IFN-β expression and activates the RIG-I/MAVS/IRF3 signaling axis in HPV-positive cervical cancer cells. (**A**) Relative expression of IFN-β mRNA in SiHa cells

following LcEV treatment. (**B**) Quantification of IFN-β secretion in the culture supernatant of SiHa cells determined by ELISA after LcEV treatment. (**C**) Relative mRNA expression levels of RIG-I, MAVS, and IRF3 in SiHa cells treated with LcEVs. (**D**) Western blot analysis of RIG-I, MAVS, and pIRF3 protein expression in SiHa cells after LcEV treatment. (**E**) Quantitative analysis of RIG-I, MAVS, and pIRF3 protein expression levels in SiHa cells. (**F**) Relative expression of IFN-β mRNA in HeLa cells following LcEV treatment. (**G**) Quantification of IFN-β secretion in the culture supernatant of HeLa cells determined by ELISA after LcEV treatment. (**H**) Relative mRNA expression levels of RIG-I, MAVS, and IRF3 in HeLa cells treated with LcEVs. (**I**) Western blot analysis of RIG-I, MAVS, and pIRF3 protein expression in HeLa cells after LcEV treatment. (**J**) Quantitative analysis of RIG-I, MAVS, and pIRF3 protein expression levels in HeLa cells. (**K**) GSEA enrichment map of GO biological processes after LcEV treatment compared with untreated cells. (**L**) Top 10 negatively enriched KEGG pathways identified by GSEA after LcEV treatment. (**M**) Top 10 positively enriched KEGG pathways identified by GSEA after LcEV treatment. Data are presented as mean ± SD. Statistical analyses were by Student's *t*-tests. * $p < 0.05$, ** $p < 0.01$, *** $p < 0.001$. Original images of 4D and 4I can be found in Supplementary File S1.

3.6. LcEV Proteomic Profiling Identifies Candidate Functional Proteins

To further explore the potential functional components responsible for the biological effects of LcEVs, we annotated the functions of 501 proteins identified from LcEVs. GO enrichment analysis revealed that LcEV-derived proteins were mainly enriched in biological processes associated with cellular response to oxidative stress, NADH metabolic processes, and ribosome biogenesis and assembly (Figure 6A). Cellular component analysis showed that identified proteins were primarily associated with ribosome-related structures, including cytosolic small ribosomal subunits, ribosomal complexes, and ribonucleoprotein complexes (Figure 6B). Molecular function analysis further demonstrated enrichment of functions related to antioxidant activity, protein disulfide oxidoreductase activity, and structural components of ribosomes (Figure 6C). Based on these functional annotations, candidate proteins with potential immunomodulatory functions were further selected for analysis. Among these proteins, thioredoxin (TrxA) was identified within the antioxidant activity category and was considered a potential candidate due to its redox regulatory properties. Additional proteins associated with immune-related functions, including GroEL, GroES, enolase, glutamine synthetase, and endopeptidase, were also selected for comparative analysis (Figure 6D). Molecular docking analysis was subsequently performed to predict the potential interaction between candidate proteins and RIG-I. The predicted binding energies varied among different candidate proteins, with TrxA showing a relatively favorable predicted binding affinity with RIG-I (Figure 6E). Structural visualization further revealed potential interaction sites between TrxA and RIG-I, including hydrogen bond interactions and amino acid residue contacts within the predicted binding interface (Figure 6F). These findings suggest that TrxA represents a potential functional protein component of LcEVs that may participate in regulating RIG-I-associated signaling responses.

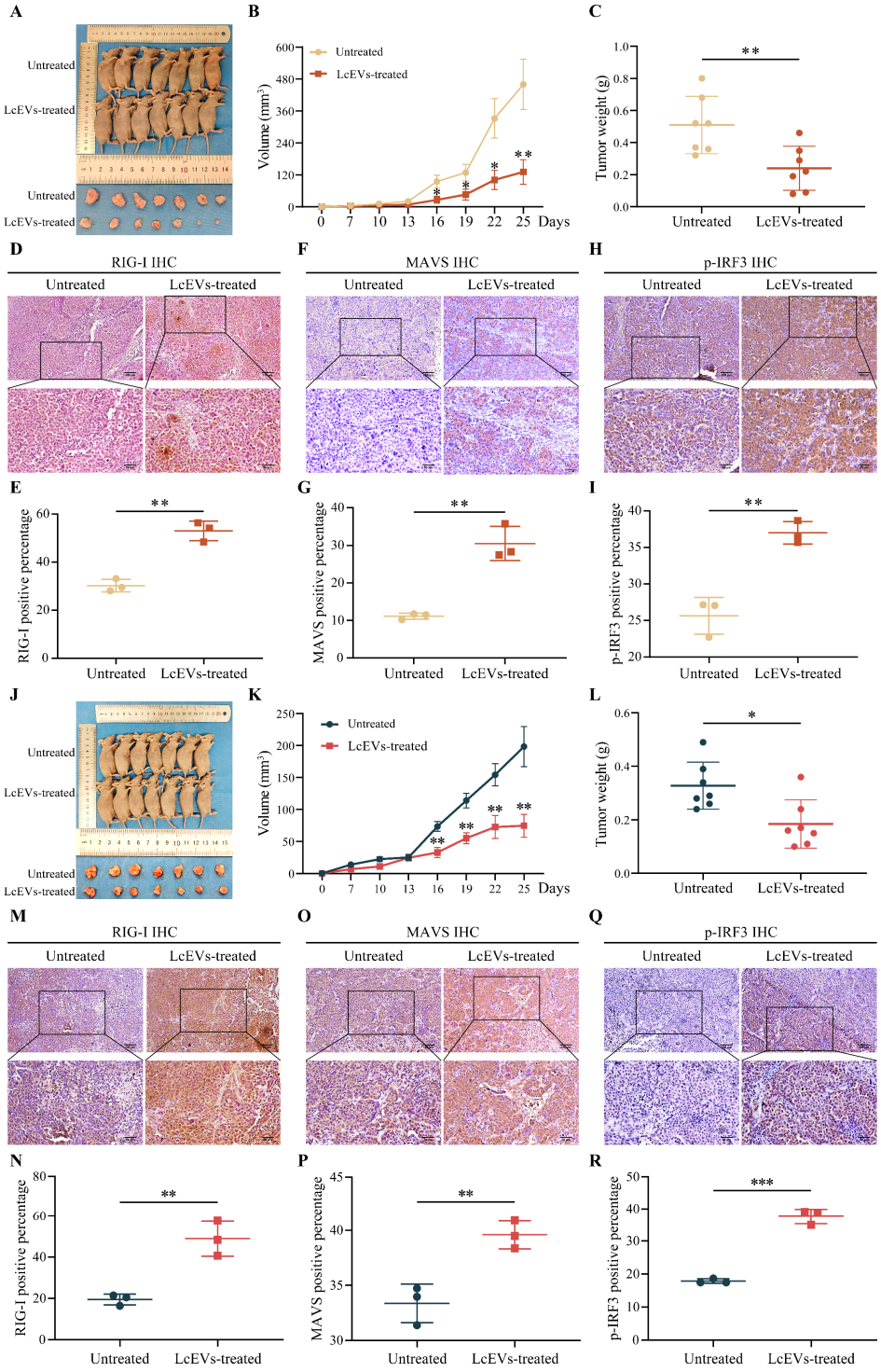
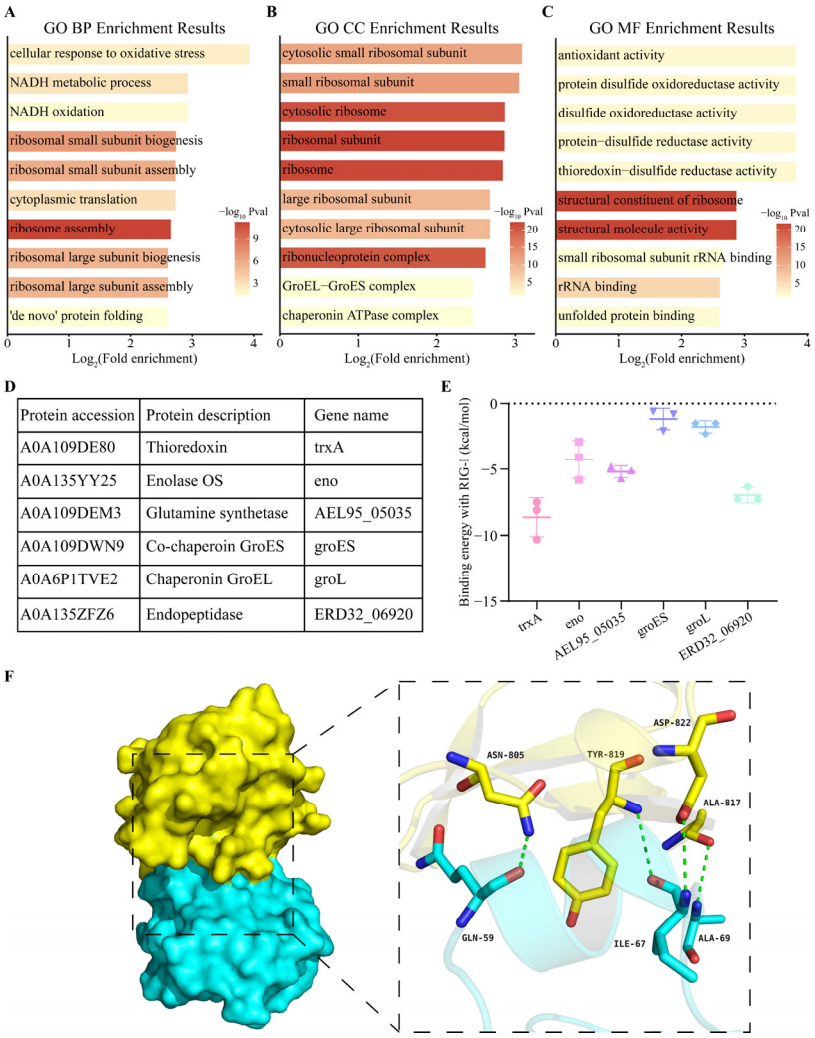


Figure 5. LcEVs suppress HPV-positive cervical cancer xenograft growth and activate the RIG-I/MAVS/IRF3 signaling axis. (**A**–**C**) Effect of LcEV treatment on tumor growth in HPV16-positive SiHa xenograft models. Representative images of mice and excised tumors, tumor growth curves, and endpoint tumor weight analysis. (**D**–**I**) Immunohistochemical analysis of RIG-I, MAVS, and p-IRF3 expression in SiHa xenograft tumor tissues. Representative IHC images and quantitative analysis of positive cells. (**J**–**L**) Effect of LcEV treatment on tumor growth in HPV18-positive HeLa xenograft models. Representative images of mice and excised tumors, tumor growth curves, and endpoint tumor weight analysis. (**M**–**R**) IHC analysis of RIG-I, MAVS, and p-IRF3 expression in HeLa xenograft tumor tissues. Representative immunohistochemical images and quantitative analysis of positive cells. Data are presented as mean ± SD. Statistical analyses were by Student's *t*-tests. * $p < 0.05$, ** $p < 0.01$, *** $p < 0.001$.



Protein accession	Protein description	Gene name
A0A109DE80	Thioredoxin	trxA
A0A135YY25	Enolase OS	eno
A0A109DEM3	Glutamine synthetase	AEL95_05035
A0A109DWN9	Co-chaperoin GroES	groES
A0A6P1TVE2	Chaperonin GroEL	groL
A0A135ZFZ6	Endopeptidase	ERD32_06920

Figure 6. Proteomic analysis of LcEVs and prediction of the potential interaction between TrxA and RIG-I. (**A**–**C**) GO enrichment analysis of LcEV-derived proteins, including BP, CC, and MF. (**D**) Annotation of selected candidate proteins with potential functional relevance. (**E**) Predicted binding energies of candidate proteins interacting with RIG-I based on molecular docking analysis. (**F**) Visualization of the predicted binding interface and interaction residues between TrxA and RIG-I.

4. Discussion

In this study, we identified *Lactobacillus crispatus* FY121-derived extracellular vesicles as a potential immunomodulatory agent against HPV-associated cervical cancer. We demonstrated that LcEVs were efficiently taken up by HPV-positive cervical cancer cells and suppressed multiple malignant phenotypes, including proliferation, migration, and invasion. Importantly, LcEVs reduced the expression of HPV E6 and E7 oncogenes and activated the RIG-I/MAVS/IRF3 signaling pathway, leading to increased IFN-β production. These findings were further supported by xenograft models, in which LcEVs inhibited tumor growth and enhanced RIG-I pathway activation in vivo. Together with proteomic characterization of LcEVs, our study provides evidence that bacterial-derived EVs can function as biologically active carriers capable of modulating tumor-associated innate immune responses. This work expands the understanding of *Lactobacillus crispatus* FY121-derived EVs beyond their traditional microbial functions and suggests a potential strategy for regulating HPV-associated tumor progression through innate immune activation.

During persistent high-risk HPV infection, viral oncoproteins not only promote malignant transformation but also impair host innate immune sensing through multiple

mechanisms. Previous studies have demonstrated that HPV16 E6 suppresses K63-linked ubiquitination of RIG-I and its interaction with MAVS through the E6-TRIM25-USP15 complex. Meanwhile, HPV16 E7 silences the promoters of RIG-I and cGAS through SUV39H1-mediated epigenetic modification and antagonizes STING-induced NF-κB activation, thereby attenuating type I interferon responses [29,30]. These findings suggest that HPV primarily establishes immune evasion by disrupting key regulatory nodes within nucleic acid sensing pathways, rather than completely eliminating the ability of host cells to respond to exogenous immune stimuli. In the present study, LcEV treatment simultaneously reduced HPV16/18 E6/E7 expression and was accompanied by increased RIG-I/MAVS protein levels, enhanced IRF3 phosphorylation, and elevated IFN-β secretion, suggesting that LcEVs may enhance RIG-I-MAVS signaling activity under the immunosuppressive conditions induced by HPV. Consistent with this observation, the RIG-I agonist M8 was reported to induce caspase-dependent apoptosis in HPV-positive cells and enhance NK cell activity [31]. In addition, intrinsic activation of RIG-I in tumor cells can induce the release of immunostimulatory EVs, which promote dendritic cell maturation and trigger T cell-dependent antitumor immunity [32]. Furthermore, following *Mycobacterium tuberculosis* infection of macrophages, bacterial RNA can be loaded into extracellular vesicles through a SecA2-dependent pathway; these vesicles are subsequently taken up by uninfected cells and activate the host RIG-I/MAVS/TBK1/IRF3 signaling axis to induce type I interferon production [27]. Based on these findings, we propose that LcEVs may reactivate the RIG-I/MAVS/IRF3 signaling axis through the delivery of exogenous RNA ligands. Activation of this pathway may enhance autocrine and paracrine IFN-β signaling, thereby limiting HPV-driven malignant phenotypes through interferon-stimulated gene (ISG)-mediated antiproliferative effects. Bacterial EVs are internalized by a broad range of host cells and modulate innate signaling through pattern recognition receptors, including TLR2-dependent activation of immune cells and macrophage polarization by *Lactobacillus plantarum* EVs [33,34]. The response to LcEVs is therefore unlikely to be restricted to HPV-positive cells, and the relative contribution of HPV-dependent and HPV-independent mechanisms remains to be defined. In HPV-positive cells, suppression of E6 and E7 provides an HPV-specific readout, whereas the effects on proliferation and migration may reflect a broader epithelial response.

Lactic acid bacteria-derived extracellular vesicles (LAB-EVs) are a class of biologically active nanoscale membrane vesicles that contain diverse functional cargos, including proteins, nucleic acids, lipids, and metabolites, and serve as important mediators of communication between microorganisms and their hosts [35]. Due to their natural origin, biocompatibility, and ability to deliver bioactive molecules, LAB-EVs have recently been considered potential postbiotic components and natural delivery platforms [36]. In the vaginal microenvironment, *Lactobacillus crispatus* is recognized as an important dominant bacterial species associated with the maintenance of a healthy microbial ecosystem. Recent studies have shown that *L. crispatus*-derived nanovesicles (nCEVs) promote tissue repair by inducing M2 macrophage polarization and inhibit vaginal HPV16 infection through the delivery of D-lactate, with stronger effects compared with vesicles derived from *Lactobacillus iners* [37]. In addition, *L. crispatus*-derived EVs have been reported to alleviate oxidative stress-induced placental cell senescence and injury by enhancing Akt phosphorylation [38]. These EVs can also reduce Helicobacter pylori-induced expression of IL-1β, IL-6, IL-8, and TNF-α while promoting the production of IL-10 and TGF-β, indicating their potential role in regulating host inflammatory responses [39]. Beyond *L. crispatus*, EVs derived from other *Lactobacillus* species have also demonstrated immunomodulatory and antitumor activities. For example, EVs derived from *Lactobacillus reuteri* can inhibit tumor cell growth and regulate apoptosis-related signaling pathways [40]. EVs from *Lactobacillus*

rhamnosus GG enhance the efficacy of anti-PD-1 therapy and promote the infiltration of $CD8^+$ T cells, $CD4^+$ T cells, and MHC II^+ dendritic cells within tumor tissues [41]. Notably, bacteria-derived EVs can also function as RNA delivery vehicles. For instance, EVs from *Legionella pneumophila* can transfer bacterial small RNAs into host cells and regulate host immune-related signaling pathways, including ddx58 (encoding RIG-I) [42]. However, previous studies have primarily focused on the effects of LAB-EVs on immune cells, inflammatory responses, and tissue homeostasis, whereas whether they can directly regulate intrinsic nucleic acid sensing processes in virus-associated tumor cells remains largely unclear. In the present study, we found that EVs derived from *Lactobacillus crispatus* FY121 were efficiently internalized by HPV16-positive SiHa cells and HPV18-positive HeLa cells and activated the RIG-I/MAVS/IRF3 signaling axis, leading to enhanced IFN-β expression and secretion. These findings suggest that LcEVs may not only serve as carriers of functional molecules but also act as natural RNA-based immunostimulatory platforms to modulate tumor cell intrinsic innate immune responses. This study further extends the understanding of LAB-EV functions in HPV-associated tumor immune regulation and provides mechanistic evidence supporting the use of probiotic-derived EVs to enhance antitumor innate immune responses.

Markers used for mammalian EVs are not encoded by bacterial genomes, and consensus marker panels for bacterial EVs have not yet been established [43–45]. Studies of *Lactobacillus* EVs have therefore characterized preparations by morphology, particle size and concentration, and protein composition [34,46,47], and the proteomic profile reported here, dominated by cytoplasmic, membrane, and cell-wall proteins, is consistent with that body of work. We acknowledge, however, that establishing a validated marker panel for *Lactobacillus* EVs remains an important goal.

The dose used here is consistent with doses reported for bacterial EVs in mucosal epithelial models. In our previous study of *S. salivarius* Ss-08 EVs, 400 μg of EV protein/mL was used for functional assays and for co-injection in vivo [48], and EVs from *Gardnerella vaginalis* and *Mobiluncus mulieris* have been applied to cervical and vaginal epithelial cells at $10^{\hat{}}7$ to $10^{\hat{}}9$ bEVs per well [49]. Xiao et al. used *L. crispatus* NCU-28 EVs at 1 mg/mL in an intrauterine adhesion model [50], and exosomes in the vaginal microenvironment have been used at $10^{\hat{}}10$ particles/mL [51]. Across eight *Lactobacillales strains*, bEV stocks ranged from $7.5 \times 10^{\hat{}}8$ to $3.2 \times 10^{\hat{}}9$ particles/mL, and protein content varied from 0.004 to 0.124 pg per particle [52]. These studies span $10^{\hat{}}7$ to $10^{\hat{}}10$ particles/mL and 0.4 to 1 mg/mL protein. The present preparation contained 2.5 × 10^11 particles/mL and more than 1000 μg protein/mL, so treatment at 400 μg of protein/mL corresponds to less than $1 \times 10^{\hat{}}11$ particles/mL. Because particle-to-protein ratios vary substantially between strains and isolation methods [52], exact dose equivalence across studies cannot be established; however, the consistency of these independent studies supports the biological plausibility of the dose used here. For a locally administered vaginal formulation, the relevant reference is the local concentration in cervicovaginal fluid rather than a systemic plasma concentration; application of a 400 μg/mL formulation in a small volume of cervicovaginal fluid would produce local exposure of the same order before clearance. This provides a realistic frame for the dose used here, while a formal pharmacokinetic measurement remains to be performed.

Several limitations should be considered when interpreting the findings of this study. First, although LcEVs contain RNA components and can be internalized by HPV-positive cervical cancer cells, it remains unclear whether vesicular RNAs are the direct effector molecules responsible for RIG-I activation. The specific RNA species with immunostimulatory activity and their molecular characteristics also remain to be identified. Second, no loss-of-function or gain-of-function experiment was performed. RIG-I or MAVS knockdown, knockout, or overexpression, and pathway inhibition were not tested, so the present data

establish an association between LcEV treatment and activation of the RIG-I/MAVS/IRF3 axis but do not show that the phenotypic effects depend on this pathway. Finally, candidate vesicular proteins, such as TrxA, identified through proteomic analysis and molecular docking currently provide mechanistic clues, but whether these proteins contribute to RIG-I regulation or function synergistically with RNA cargoes remains to be experimentally validated. Future studies will further clarify the mechanistic basis and translational potential of LcEVs as microbiota-derived innate immune modulators for the intervention of HPV-associated cervical lesions.

5. Conclusions

In conclusion, this study shows that extracellular vesicles derived from *Lactobacillus crispatus* FY121 reduce the viability, migration, and invasion of HPV-positive cervical cancer cells lines and suppress HPV16/18 E6/E7 expression and that these effects are accompanied by activation of the RIG-I/MAVS/IRF3 signaling axis and increased IFN-β responses. These findings extend the biological significance of *Lactobacillus*-derived EVs beyond conventional roles in microbial–host communication and immune homeostasis, suggesting that LcEVs may function as natural immunostimulatory nanocarriers capable of modulating tumor cell intrinsic innate immune sensing. The cargo responsible for these effects and the requirement for RIG-I/MAVS signaling were not defined in the present study, and the signaling changes reported here should therefore be read as an association that provides a basis for further mechanistic work.

Supplementary Materials: The following supporting information can be downloaded at: https://www.mdpi.com/article/10.3390/biom16111560/s1, Figure S1: Characterization of LcEVs derived from *Lactobacillus crispatus* FY121. Supplementary File S1: Original western blot images for Figures 3C,G and 4D,I.

Author Contributions: Conceptualization: Y.F.; Methodology: G.C., S.L. and Y.F.; Investigation: G.C. and S.L.; Formal analysis: G.C. and S.L.; Data curation: G.C., S.L. and L.L.; Software: G.C.; Writing—original draft: G.C.; Writing—review and editing: G.C., S.L. and Y.F.; Validation: M.Y., C.X., M.D. and L.L.; Resources: Y.F.; Supervision: Y.F.; Project administration: Y.F.; Funding acquisition: Y.F. and S.L. All authors have read and agreed to the published version of the manuscript.

Funding: This work was supported by the 2025 Heilongjiang Province "Double First-Class" Discipline Collaborative Innovation Achievement Project (LJGXCG2025-P10) and the Heilongjiang Provincial Health Commission Research Project (20251212060510).

Institutional Review Board Statement: The animal study protocol was approved by the Ethics Committee of Harbin Medical University (protocol code: HMUIRB2026037; 30 June 2026).

Informed Consent Statement: Not applicable.

Data Availability Statement: The proteomics data are available in the PRIDE repository under accession number PXD051142. The RNA-seq count and FPKM matrices are provided in the Supplementary Materials. Further information is available from the corresponding author upon reasonable request.

Conflicts of Interest: The authors declare no competing interests.

References

1. Olawaiye, A.B.; Baker, T.P.; Washington, M.K.; Mutch, D.G. The new (Version 9) American Joint Committee on Cancer tumor, node, metastasis staging for cervical cancer. *CA Cancer J. Clin.* **2021**, *71*, 287–298. [CrossRef] [PubMed]
2. Yang, A.; Farmer, E.; Wu, T.C.; Hung, C.F. Perspectives for therapeutic HPV vaccine development. *J. Biomed. Sci.* **2016**, *23*, 75. [CrossRef] [PubMed]

3. Fontham, E.T.H.; Wolf, A.M.D.; Church, T.R.; Etzioni, R.; Flowers, C.R.; Herzig, A.; Guerra, C.E.; Oeffinger, K.C.; Shih, Y.T.; Walter, L.C.; et al. Cervical cancer screening for individuals at average risk: 2020 guideline update from the American Cancer Society. *CA Cancer J. Clin.* **2020**, *70*, 321–346. [CrossRef] [PubMed]
4. Pal, A.; Kundu, R. Human Papillomavirus E6 and E7: The Cervical Cancer Hallmarks and Targets for Therapy. *Front. Microbiol.* **2019**, *10*, 3116. [CrossRef] [PubMed]
5. Ni, H.; Huang, C.; Ran, Z.; Li, S.; Kuang, C.; Zhang, Y.; Yuan, K. Targeting HPV for the prevention, diagnosis, and treatment of cervical cancer. *J. Mol. Cell Biol.* **2025**, *16*, mjae046. [CrossRef] [PubMed]
6. Upadhyay, S.; Nagampalli, R.; Resende, S.; Kanneganti, T.D. Innate immune sensors of inflammasomes and PANoptosomes: Structural-mechanistic insights and therapeutic implications. *Cell Res.* **2026**, *36*, 747–768. [CrossRef] [PubMed]
7. Yu, X.; Jin, Y.; Li, B.; Deng, J.; Zhou, Y.; Zhang, J.; Li, H. DAMPs, PAMPs, and Alarmins: From Mechanism to Therapy. *MedComm* **2026**, *7*, e70923. [CrossRef] [PubMed]
8. Zhu, Q.; Yu, S. The role of cGAS-STING signaling in HPV infection and HPV-related cancers. *Front. Immunol.* **2025**, *16*, 1709613. [CrossRef] [PubMed]
9. Chen, H.M.; Zhang, J.; Li, J.X.; Li, C.H.; Li, Y.F.; Zhang, Q.; Kong, B.; Wang, P.H. The viral early protein 4 of human papillomavirus type 16 suppresses innate antiviral immunity. *Int. J. Biol. Macromol.* **2025**, *315*, 144542. [CrossRef] [PubMed]
10. Li, J.X.; Zhang, J.; Li, C.H.; Li, Y.F.; Chen, H.M.; Li, T.; Zhang, Q.; Kong, B.H.; Wang, P.H. Human papillomavirus E1 proteins inhibit RIG-I/MDA5-MAVS, TLR3-TRIF, cGAS-STING, and JAK-STAT signaling pathways to evade innate antiviral immunity. *Front. Immunol.* **2025**, *16*, 1549766. [CrossRef] [PubMed]
11. Li, J.X.; Zhang, J.; Li, C.H.; Zhang, Q.; Kong, B.; Wang, P.H. Human papillomavirus E2 proteins suppress innate antiviral signaling pathways. *Front. Immunol.* **2025**, *16*, 1555629. [CrossRef] [PubMed]
12. Bortnik, V.; Wu, M.; Julcher, B.; Salinas, A.; Nikolic, I.; Simpson, K.J.; McMillan, N.A.; Idris, A. Loss of HPV type 16 E7 restores cGAS-STING responses in human papilloma virus-positive oropharyngeal squamous cell carcinomas cells. *J. Microbiol. Immunol. Infect. = Wei Mian Yu Gan Ran Za Zhi* **2021**, *54*, 733–739. [CrossRef] [PubMed]
13. Yoneyama, M.; Kato, H.; Fujita, T. Physiological functions of RIG-I-like receptors. *Immunity* **2024**, *57*, 731–751. [CrossRef] [PubMed]
14. van Huizen, M.; Gack, M.U. The RIG-I-like receptor family of immune proteins. *Mol. Cell* **2025**, *85*, 3793–3806. [CrossRef] [PubMed]
15. Naumann, M.; Wierschin, T.M.; Kretschmer, S.; Dash, B.P.; Held, A.; Salzinger, A.; Peikert, K.; Karlek, A.; Glaß, H.; Großmann, D.; et al. RIG-I Mediated Neuron-Specific IFN Type 1 Signaling in FUS-ALS Induces Neurodegeneration and Offers New Biomarker-Driven Individualized Treatment Options for (FUS-)ALS. *Adv. Sci.* **2026**, *13*, e17135. [CrossRef] [PubMed]
16. Heidegger, S.; Wintges, A.; Stritzke, F.; Bek, S.; Steiger, K.; Koenig, P.A.; Göttert, S.; Engleitner, T.; Öllinger, R.; Nedelko, T.; et al. RIG-I activation is critical for responsiveness to checkpoint blockade. *Sci. Immunol.* **2019**, *4*, eaau8943. [CrossRef] [PubMed]
17. Gill, S.; Catchpole, R.; Forterre, P. Extracellular membrane vesicles in the three domains of life and beyond. *FEMS Microbiol. Rev.* **2019**, *43*, 273–303. [CrossRef] [PubMed]
18. Woith, E.; Fuhrmann, G.; Melzig, M.F. Extracellular Vesicles-Connecting Kingdoms. *Int. J. Mol. Sci.* **2019**, *20*, 5695. [CrossRef] [PubMed]
19. McMillan, H.M.; Kuehn, M.J. The extracellular vesicle generation paradox: A bacterial point of view. *EMBO J.* **2021**, *40*, e108174. [CrossRef] [PubMed]
20. Turnbull, L.; Toyofuku, M.; Hynen, A.L.; Kurosawa, M.; Pessi, G.; Petty, N.K.; Osvath, S.R.; Cárcamo-Oyarce, G.; Gloag, E.S.; Shimoni, R.; et al. Explosive cell lysis as a mechanism for the biogenesis of bacterial membrane vesicles and biofilms. *Nat. Commun.* **2016**, *7*, 11220. [CrossRef] [PubMed]
21. Ñahui Palomino, R.A.; Vanpouille, C.; Costantini, P.E.; Margolis, L. Microbiota-host communications: Bacterial extracellular vesicles as a common language. *PLoS Pathog.* **2021**, *17*, e1009508. [CrossRef] [PubMed]
22. Xie, J.; Li, Q.; Haesebrouck, F.; Van Hoecke, L.; Vandenbroucke, R.E. The tremendous biomedical potential of bacterial extracellular vesicles. *Trends Biotechnol.* **2022**, *40*, 1173–1194. [CrossRef] [PubMed]
23. Chronopoulos, A.; Kalluri, R. Emerging role of bacterial extracellular vesicles in cancer. *Oncogene* **2020**, *39*, 6951–6960. [CrossRef] [PubMed]
24. Liang, A.; Korani, L.; Yeung, C.L.S.; Tey, S.K.; Yam, J.W.P. The emerging role of bacterial extracellular vesicles in human cancers. *J. Extracell. Vesicles* **2024**, *13*, e12521. [CrossRef] [PubMed]
25. Ñahui Palomino, R.A.; Vanpouille, C.; Laghi, L.; Parolin, C.; Melikov, K.; Backlund, P.; Vitali, B.; Margolis, L. Extracellular vesicles from symbiotic *vaginal lactobacilli* inhibit HIV-1 infection of human tissues. *Nat. Commun.* **2019**, *10*, 5656. [CrossRef] [PubMed]
26. Steinman, D.; Petersen, A.P.; Chibber, Y.; Crawford, C.; Tyagi, P.; Zierden, H.C. Vaginal bacteria-derived extracellular vesicles diffuse through human cervicovaginal mucus to enable microbe-host signaling. *npj Biofilms Microbiomes* **2026**, *12*, 10. [CrossRef] [PubMed]

27. Cheng, Y.; Schorey, J.S. Extracellular vesicles deliver *Mycobacterium* RNA to promote host immunity and bacterial killing. *EMBO Rep.* **2019**, *20*, EMBR201846613. [CrossRef] [PubMed]
28. Tang, D.; Chen, M.; Huang, X.; Zhang, G.; Zeng, L.; Zhang, G.; Wu, S.; Wang, Y. SRplot: A free online platform for data visualization and graphing. *PLoS ONE* **2023**, *18*, e0294236. [CrossRef] [PubMed]
29. Chiang, C.; Pauli, E.K.; Biryukov, J.; Feister, K.F.; Meng, M.; White, E.A.; Münger, K.; Howley, P.M.; Meyers, C.; Gack, M.U. The Human Papillomavirus E6 Oncoprotein Targets USP15 and TRIM25 To Suppress RIG-I-Mediated Innate Immune Signaling. *J. Virol.* **2018**, *92*, e01737-17. [CrossRef] [PubMed]
30. Lo Cigno, I.; Calati, F.; Borgogna, C.; Zevini, A.; Albertini, S.; Martuscelli, L.; De Andrea, M.; Hiscott, J.; Landolfo, S.; Gariglio, M. Human Papillomavirus E7 Oncoprotein Subverts Host Innate Immunity via SUV39H1-Mediated Epigenetic Silencing of Immune Sensor Genes. *J. Virol.* **2020**, *94*, e01812-19. [CrossRef] [PubMed]
31. Girone, C.; Calati, F.; Lo Cigno, I.; Salvi, V.; Tassinari, V.; Schioppa, T.; Borgogna, C.; Lospinoso Severini, L.; Hiscott, J.; Cerboni, C.; et al. The RIG-I agonist M8 triggers cell death and natural killer cell activation in human papillomavirus-associated cancer and potentiates cisplatin cytotoxicity. *Cancer Immunol. Immunother. CII* **2023**, *72*, 3097–3110. [CrossRef] [PubMed]
32. Heidegger, S.; Stritzke, F.; Dahl, S.; Daßler-Plenker, J.; Joachim, L.; Buschmann, D.; Fan, K.; Sauer, C.M.; Ludwig, N.; Winter, C.; et al. Targeting nucleic acid sensors in tumor cells to reprogram biogenesis and RNA cargo of extracellular vesicles for T cell-mediated cancer immunotherapy. *Cell Rep. Med.* **2023**, *4*, 101171. [CrossRef] [PubMed]
33. Morishita, M.; Sagayama, R.; Yamawaki, Y.; Yamaguchi, M.; Katsumi, H.; Yamamoto, A. Activation of Host Immune Cells by Probiotic-Derived Extracellular Vesicles via TLR2-Mediated Signaling Pathways. *Biol. Pharm. Bull.* **2022**, *45*, 354–359. [CrossRef] [PubMed]
34. Kim, W.; Lee, E.J.; Bae, I.H.; Myoung, K.; Kim, S.T.; Park, P.J.; Lee, K.H.; Pham, A.V.Q.; Ko, J.; Oh, S.H.; et al. *Lactobacillus plantarum*-derived extracellular vesicles induce anti-inflammatory M2 macrophage polarization in vitro. *J. Extracell. Vesicles* **2020**, *9*, 1793514. [CrossRef] [PubMed]
35. Li, M.; Mao, B.; Tang, X.; Zhang, Q.; Zhao, J.; Chen, W.; Cui, S. Lactic acid bacteria derived extracellular vesicles: Emerging bioactive nanoparticles in modulating host health. *Gut Microbes* **2024**, *16*, 2427311. [CrossRef] [PubMed]
36. Liu, Y. Recent advances in lactic acid bacteria-derived extracellular vesicles. *Curr. Opin. Microbiol.* **2026**, *93*, 102819. [CrossRef] [PubMed]
37. Peng, K.; Chen, X.; Zhang, Y.; Liu, L.; Huang, Q.; Du, S.; Zhu, C.; Wang, Y.; Wei, F.; Gao, S.; et al. *Lactobacillus crispatus*-derived nCEV vesicles promote cutaneous wound healing and inhibit HPV16 infection. *mSystems* **2025**, *10*, e0068325. [CrossRef] [PubMed]
38. Wang, L.-M.; Lee, B.-H.; Hou, C.-Y.; Hsu, W.-H.; Tai, C.-J. Probiotics-Derived Extracellular Vesicles Protect Oxidative Stress against H2O2 Induction in Placental Cells. *Fermentation* **2022**, *8*, 74. [CrossRef]
39. Fakharian, F.; Sadeghi, A.; Pouresmaeili, F.; Soleimani, N.; Yadegar, A. Anti-inflammatory effects of extracellular vesicles and cell-free supernatant derived from *Lactobacillus crispatus* strain RIGLD-1 on Helicobacter pylori-induced inflammatory response in gastric epithelial cells in vitro. *Folia Microbiol.* **2024**, *69*, 927–939. [CrossRef] [PubMed]
40. Yi, S.; Jung, E.; Kim, H.; Choi, J.; Kim, S.; Lim, E.K.; Kim, K.S.; Kang, T.; Jung, J. Harnessing *Lactobacillus reuteri*-Derived Extracellular Vesicles for Multifaceted Cancer Treatment. *Small* **2025**, *21*, e2406094. [CrossRef] [PubMed]
41. Lu, S.; Xu, J.; Zhao, Z.; Guo, Y.; Zhang, H.; Jurutka, P.W.; Huang, D.; Cao, C.; Cheng, S. *Dietary Lactobacillus rhamnosus* GG extracellular vesicles enhance antiprogrammed cell death 1 (anti-PD-1) immunotherapy efficacy against colorectal cancer. *Food Funct.* **2023**, *14*, 10314–10328. [CrossRef] [PubMed]
42. Sahr, T.; Escoll, P.; Rusniok, C.; Bui, S.; Pehau-Arnaudet, G.; Lavieu, G.; Buchrieser, C. Translocated *Legionella pneumophila* small RNAs mimic eukaryotic microRNAs targeting the host immune response. *Nat. Commun.* **2022**, *13*, 762. [CrossRef] [PubMed]
43. Welsh, J.A.; Goberdhan, D.C.I.; O'Driscoll, L.; Buzas, E.I.; Blenkiron, C.; Bussolati, B.; Cai, H.; Di Vizio, D.; Driedonks, T.A.P.; Erdbrügger, U.; et al. Minimal information for studies of extracellular vesicles (MISEV2023): From basic to advanced approaches. *J. Extracell. Vesicles* **2024**, *13*, e12404. [CrossRef] [PubMed]
44. Erdbrügger, U.; Blijdorp, C.J.; Bijnsdorp, I.V.; Borràs, F.E.; Burger, D.; Bussolati, B.; Byrd, J.B.; Clayton, A.; Dear, J.W.; Falcón-Pérez, J.M.; et al. Urinary extracellular vesicles: A position paper by the Urine Task Force of the International Society for Extracellular Vesicles. *J. Extracell. Vesicles* **2021**, *10*, e12093. [CrossRef] [PubMed]
45. Choi, D.; Lee, E.Y. Standardizing Bacterial Extracellular Vesicle Purification: A Call for Consensus. *J. Microbiol. Biotechnol.* **2025**, *35*, e2506011. [CrossRef] [PubMed]
46. Huang, J.; Zhao, A.; He, D.; Wu, X.; Yan, H.; Zhu, L. Isolation and Proteomic Analysis of Extracellular Vesicles from *Lactobacillus salivarius* SNK-6. *J. Microbiol. Biotechnol.* **2024**, *34*, 224–231. [CrossRef] [PubMed]
47. Wang, H.; Sim, J.; Jeong, A.H.; Kim, H.; Im, Y.; Roh, K.B.; Jung, E.; Park, D.; Cho, E. Functional and proteomic analysis of *Lactobacillus rhamnosus*-derived extracellular vesicles with antioxidant and anti-inflammatory activity. *Sci. Rep.* **2025**, *16*, 3124. [CrossRef] [PubMed]
48. Cao, G.; Yuan, M.; Ding, M.; Jiang, Y.; Xue, C.; Fang, Y. *Streptococcus salivarius* Ss-08 Extracellular Vesicles Suppress OSCC Progression via Inhibition of JAG1-NOTCH1 Signaling. *Int. J. Mol. Sci.* **2026**, *27*, 7595. [CrossRef] [PubMed]

49. Joseph, A.; Anton, L.; Guan, Y.; Ferguson, B.; Mirro, I.; Meng, N.; France, M.; Ravel, J.; Elovitz, M.A. Extracellular vesicles from vaginal *Gardnerella vaginalis* and *Mobiluncus mulieris* contain distinct proteomic cargo and induce inflammatory pathways. *npj Biofilms Microbiomes* **2024**, *10*, 28. [CrossRef] [PubMed]
50. Xiao, Q.; Ding, L.; Zhang, X.; Liu, C.; Li, Y.; Xu, R.; Li, Q.; Ji, M.; Wei, J.; Chen, T.; et al. Extracellular vesicles ameliorate intrauterine adhesion through Nrf2/GPX4-mediated ferroptosis suppression. *J. Adv. Res.* **2026**. *Epub ahead of printing*. [CrossRef] [PubMed]
51. Wang, L.M.; Shi, Y.C.; Lee, B.H.; Liu, C.H.; Loh, E.W.; Tai, C.J.; Lin, L.T. LPS-induced endometrial cell-derived exosomes suppress probiotic *Lactobacillus* growth. *Sci. Rep.* **2026**, *16*, 15301. [CrossRef] [PubMed]
52. Park, S.; Mok, J.; Yu, H.M.; An, H.J.; Choi, G.H.; Lee, Y.S.; Kwon, K.J.; Choi, S.J.; Kim, K.H.; Kim, S.J.; et al. Comparative and pharmacological investigation of bEVs from eight *Lactobacillales* strains. *Sci. Rep.* **2025**, *15*, 27263. [CrossRef] [PubMed]

Disclaimer/Publisher's Note: The statements, opinions and data contained in all publications are solely those of the individual author(s) and contributor(s) and not of MDPI and/or the editor(s). MDPI and/or the editor(s) disclaim responsibility for any injury to people or property resulting from any ideas, methods, instructions or products referred to in the content.